

Boundary conditions for light propagation in diffusive media with nonscattering regions

Jorge Ripoll and Manuel Nieto-Vesperinas

Instituto de Ciencia de Materiales de Madrid, Consejo Superior de Investigaciones Científicas, Campus de Cantoblanco, 28049 Madrid, Spain

Simon R. Arridge and Hamid Dehghani

Department of Computer Science, University College London, Gower Street, London, WC1 E6BT, UK

Received November 2, 1999; revised manuscript received May 8, 2000; accepted May 11, 2000

The diffusion approximation proves to be valid for light propagation in highly scattering media, but it breaks down in the presence of nonscattering regions. We present a compact expression of the boundary conditions for diffusive media with nonscattering regions, taking into account small-index mismatch. Results from an integral method based on the extinction theorem boundary condition are contrasted with both Monte Carlo and finite-element-method simulations, and a study of its limit of validity is presented. These procedures are illustrated by considering the case of the cerebro-spinal fluid in the brain, for which we demonstrate that for practical situations in light diffusion, these boundary conditions yield accurate results. © 2000 Optical Society of America [S0740-3232(00)00409-9]

OCIS codes: 170.5270, 290.1990.

1. INTRODUCTION

The study of light propagation through strongly scattering media has received increasing attention during the past few years, partly as a result of its applications to medical diagnosis.^{1,2} In many practical situations it has been shown that visible or near-infrared light transport within turbid media such as human tissues³ can be adequately modeled by the diffusion equation, on the basis of which several imaging methods have been analyzed^{4–20} (see Ref. 20 for a review on the subject of optical tomography). Specifically, much research is motivated by the ability of optical radiation to diagnose brain tumors. However, a problem arises in studying complex systems such as the brain, in which not all regions diffuse light. These cases are those in which new boundary conditions that model the interaction of the diffuse light with non-diffusive media are needed.^{21–24}

Many studies have been published concerning the way to correctly model the diffuse–nondiffuse interface when the scattered light is detected from outside the diffusive medium.^{25–36} The diffusion approximation does not hold near nondiffuse interfaces, and to date there exists no closed correct expression for such boundary conditions. Even so, it has been shown that in a nonscattering region embedded in a diffuse medium (for instance, an air bubble in milk), the diffusion approximation, in combination with the radiative transfer equation (RTE) in a nonscattering medium, can still yield correct results^{21,22}: That is, light propagation can still be accurately modeled by the diffusion approximation when light incident on the nonscattering region is already diffuse. An important instance of a biological medium with this type of region is the brain, which is mostly a scatterer except for those regions filled with cerebro-spinal fluid. The limit of valid-

ity of such an approximation will depend both on the ratio between the scattering and the nonscattering volumes and on the refractive index. Therefore a closed expression for the boundary conditions in such media is needed for correct modeling of the interaction at such interfaces.

Following previous studies in which advances in this subject were made,^{21,22} we present a compact expression of the boundary conditions for diffusive media with nonscattering regions. To obtain the expression for these boundary conditions, we make use of the RTE,³⁷ on which the diffusion approximation is based. To enhance the clarity and comprehensiveness of the steps followed, in Section 2 we concisely revise the main facts of the RTE, both in free space and in a diffusive medium. Then in Section 3 we derive the expression for the boundary conditions on the basis of the theory presented in Section 2. Further, we present the scattering integral equations, which include the interaction of the incident wave front of diffuse light with a nonscattering region by means of these boundary conditions. In Section 4 we present rigorous numerical results for the corresponding system of integral equations, solved by means of the extinction theorem (ET) integral method,^{38–40} which, when applied both above and below the interface, yields the nonlocal boundary values for both the average intensity and its normal derivative. The ET method enables one to include any type of mixed boundary conditions and to solve them without any approximation. We compare results derived from the ET with those obtained with the finite-element model^{41–43} (FEM), which takes into account the nonscattering medium by approximating the boundary conditions. Both methods are then contrasted with Monte Carlo (MC) simulations, and the advantages of using one or another procedure are discussed accordingly.

Results are put forward for two distinct situations: the case of a cylindrical nonscattering region embedded in a diffusive cylinder and the case of a cylindrical nonscattering gap embedded in a diffusive cylinder. We discuss the limit of validity of the boundary conditions established in this work by considering the influence of the nonscattering volume versus that of the diffusive volume. Finally, in Section 5 we summarize the main conclusions.

2. GENERAL EXPRESSIONS OF THE RADIATIVE TRANSFER EQUATION

For comprehensiveness and clarity in order to arrive at the desired expression of the boundary conditions for diffuse–nondiffuse interfaces, we summarize in this section the main facts of the theory of the RTE. We follow the notation used in Ref. 37, where a detailed account can be found.

A way of characterizing the light flow of energy and its interaction with the medium is by means of the specific intensity $I(\mathbf{r}, \hat{\mathbf{s}})$, which represents the average power flux at point \mathbf{r} that flows in the direction $\hat{\mathbf{s}}$ and has units [$W\text{ cm}^{-2}\text{ sr}^{-1}$]. In terms of the specific intensity, the average intensity U and the total flux density \mathbf{J} are defined as

$$U(\mathbf{r}) = \int_{4\pi} I(\mathbf{r}, \hat{\mathbf{s}}) d\Omega, \quad (1)$$

$$\mathbf{J}(\mathbf{r}) = \int_{4\pi} I(\mathbf{r}, \hat{\mathbf{s}}) \hat{\mathbf{s}} d\Omega, \quad (2)$$

where both U and \mathbf{J} have units of watts per square centimeter and $d\Omega$ is the solid-angle element $d\Omega = d\phi \sin\theta d\theta$. The total flux density that flows through a differential area $d\mathbf{S} = \hat{\mathbf{n}} dS$ is then

$$J_n(\mathbf{r}) = \mathbf{J}(\mathbf{r}) \cdot \hat{\mathbf{n}} = \int_{4\pi} I(\mathbf{r}, \hat{\mathbf{s}}) \hat{\mathbf{n}} \cdot \hat{\mathbf{s}} d\Omega, \quad (3)$$

where $\hat{\mathbf{n}}$ is the unit outward normal to the area element dS . Therefore the amount of power dp emitted from $d\mathbf{S}$ in the direction of the unit vector $\hat{\mathbf{s}}$ and flowing within a solid angle $d\Omega$ can be written as

$$dp(\mathbf{r}, \hat{\mathbf{s}}) = I(\mathbf{r}, \hat{\mathbf{s}}) \hat{\mathbf{n}} \cdot \hat{\mathbf{s}} dS d\Omega, \quad (4)$$

is in units of watts. Then the total power emitted from $d\mathbf{S}$ would be

$$dP(\mathbf{r}) = \int_{4\pi} dp(\mathbf{r}, \hat{\mathbf{s}}) = \int_{4\pi} I(\mathbf{r}, \hat{\mathbf{s}}) \hat{\mathbf{n}} \cdot \hat{\mathbf{s}} dS d\Omega = J_n(\mathbf{r}) dS, \quad (5)$$

which is measured in watts. Let the area S separate two different media with different refractive indices (see Fig. 1): an upper medium with refractive index n_0 and a lower medium with refractive index n_1 . Then we can write the total downward J^- and upward J^+ fluxes through $d\mathbf{S}$ by means of Eq. (2) as

$$J^+(\mathbf{r}) = \int_{(2\pi)^+} I_{1 \rightarrow 0}^i(\mathbf{r}, \hat{\mathbf{s}}) \hat{\mathbf{s}} \cdot \hat{\mathbf{n}} d\Omega, \quad (6)$$

$$J^-(\mathbf{r}) = \int_{(2\pi)^-} I_{0 \rightarrow 1}^i(\mathbf{r}, -\hat{\mathbf{s}}) (-\hat{\mathbf{s}} \cdot \hat{\mathbf{n}}) d\Omega, \quad (7)$$

where $I_{i \rightarrow j}^i$ represents the specific intensity transmitted on going from medium i into medium j . Their net flux through $d\mathbf{S}$ is therefore $J_n(\mathbf{r}) = J^+(\mathbf{r}) - J^-(\mathbf{r})$. In terms of conservation of power, we can then write the total incident power at $d\mathbf{S}$ as a sum of the reflected and transmitted powers; i.e.,

$$dp^i(\mathbf{r}, \theta_i) = dp^r(\mathbf{r}, \theta_r) + dp^t(\mathbf{r}, \theta_t), \quad (8)$$

where

$$dp^r(\mathbf{r}, \theta_t) = R_p(\theta_i) dp^i(\mathbf{r}, \theta_i), \quad (9)$$

$$dp^t(\mathbf{r}, \theta_t) = [1 - R_p(\theta_i)] dp^i(\mathbf{r}, \theta_i). \quad (10)$$

In Eqs. (9) and (10) R_p is the power reflectivity, which in terms of the Fresnel reflection coefficients is given by $R_p = |R|^2$, where R actually denotes R_{\parallel} or R_{\perp} depending on whether the polarization is TM or TE. If the wave is completely unpolarized, then $|R|^2$ should be equal to $1/2(|R_{\parallel}|^2 + |R_{\perp}|^2)$. By means of the relationship shown in Eqs. (5), (8), and (10), we can rewrite Eqs. (6) and (7) as

$$J^+(\mathbf{r}) = \int_{(2\pi)^-} [1 - |R_{1 \rightarrow 0}(\theta_i)|^2] I_1(\mathbf{r}, \hat{\mathbf{s}}) \hat{\mathbf{s}} \cdot \hat{\mathbf{n}} d\Omega_i, \quad (11)$$

$$J^-(\mathbf{r}) = \int_{(2\pi)^+} [1 - |R_{0 \rightarrow 1}(\theta_i)|^2] I_0(\mathbf{r}, -\hat{\mathbf{s}}) (-\hat{\mathbf{s}} \cdot \hat{\mathbf{n}}) d\Omega_i, \quad (12)$$

where I_0 and I_1 represent the specific intensities incident on S from medium 0 and 1, respectively. It should be noticed that owing to the relationships between dp^t and dp^i through the Fresnel coefficients, Eqs. (9) and (10), the integration in Eqs. (11) and (12) is performed over the incident angles, whereas in Eqs. (6) and (7) the integration was done over the transmitted angles. That is, in Eqs. (11) and (12), $R_{i \rightarrow j}(\theta_i)$ represents the reflection coefficient corresponding to the angle of incidence θ_i on going to medium j from medium i , and $d\Omega_i = d\phi_i \sin\theta_i d\theta_i$. Also, Eqs. (11) and (12) are general for the RTE, since the scat-

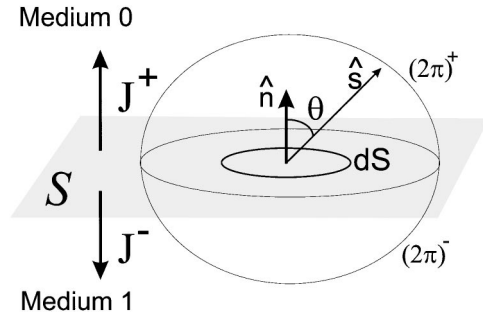


Fig. 1. Schematic view of the geometry with the upward (\mathbf{J}^+) and downward (\mathbf{J}^-) density flux at an interface.

tering or absorbing specific properties of medium 0 and 1 have not yet been introduced.

A. Nonscattering Medium

The expression for the RTE in a nonscattering medium is³⁷

$$\frac{n}{c} \frac{\partial I(\mathbf{r}, \hat{\mathbf{s}})}{\partial t} + \hat{\mathbf{s}} \cdot \nabla I(\mathbf{r}, \hat{\mathbf{s}}) + \mu_a I(\mathbf{r}, \hat{\mathbf{s}}) = 0, \quad (13)$$

where μ_a is the absorption coefficient of the nonscattering medium, is in units of inverse centimeters; n is the refractive index; and c is the speed of light in vacuum. For a continuous source located at \mathbf{r}' , i.e., with no temporal dependence, the solution to Eq. (13) is

$$I(\mathbf{r}, \hat{\mathbf{u}}_{\mathbf{r}-\mathbf{r}'}) = I(\mathbf{r}', \hat{\mathbf{u}}_{\mathbf{r}'-\mathbf{r}}) \exp[-\mu_a |\mathbf{r} - \mathbf{r}'|], \quad (14)$$

where $\hat{\mathbf{u}}_{\mathbf{r}-\mathbf{r}'} = (\mathbf{r} - \mathbf{r}')/|\mathbf{r} - \mathbf{r}'|$. With reference to the configuration depicted in Fig. 1, consider the case in which the surface S separates the nonscattering inner medium (medium 0) with refractive index n_0 and absorption coefficient μ_{a0} , from the outer medium (medium 1) with refractive index n_1 , which can be either scattering or nonscattering. The amount of power incident on the elementary area $d\mathbf{S} \in S$ located at point \mathbf{r} and emitted from the elementary area $d\mathbf{S}' \in S$ located at \mathbf{r}' (see Fig. 2) will be

$$dP^i(\mathbf{r}, \theta) = I_0(\mathbf{r}', \hat{\mathbf{u}}_{\mathbf{r}'-\mathbf{r}}) \exp[-\mu_{a0} |\mathbf{r} - \mathbf{r}'|] \cos \theta dS d\Omega, \quad (15)$$

where $\cos \theta = \mathbf{n} \cdot \hat{\mathbf{u}}_{\mathbf{r}-\mathbf{r}'}$ and I_0 represents the specific intensity inside the nonscattering volume. Note that we consider S to be the union of all surfaces contributing to the flux at \mathbf{r} , which in general may have a complex topology; see Ref. 22 for further discussion of this topic. The total power transmitted at \mathbf{r} , taking all possible incidence angles into consideration, is [see Eq. (10)]

$$dP^t(\mathbf{r}) = \int_{(2\pi)^+} (1 - |R_{0 \rightarrow 1}(\theta)|^2) I_0(\mathbf{r}', \hat{\mathbf{u}}_{\mathbf{r}-\mathbf{r}'}) \times \exp[-\mu_{a0} |\mathbf{r} - \mathbf{r}'|] \hat{\mathbf{n}} \cdot \hat{\mathbf{u}}_{\mathbf{r}-\mathbf{r}'} dS d\Omega. \quad (16)$$

By using the fact that $d\Omega = d\mathbf{S}' \cdot \hat{\mathbf{u}}_{\mathbf{r}-\mathbf{r}'}/|\mathbf{r} - \mathbf{r}'|^2$ (see Fig. 2), and $J^-(\mathbf{r}) = dP^t(\mathbf{r})/dS$ [see Eq. (5)], we write the total flux density transmitted through every point \mathbf{r} of S in terms of the specific intensity radiated by the complete surface as

$$J^-(\mathbf{r}) = \int_S I_0(\mathbf{r}', \hat{\mathbf{u}}_{\mathbf{r}-\mathbf{r}'}) \mathcal{G}(\mathbf{r} - \mathbf{r}') dS', \quad \mathbf{r} \in S, \quad (17)$$

where we have defined

$$\mathcal{G}(\mathbf{r} - \mathbf{r}') = [1 - |R_{0 \rightarrow 1}(\theta)|^2] \frac{\exp[-\mu_{a0} |\mathbf{r} - \mathbf{r}'|]}{|\mathbf{r} - \mathbf{r}'|^2} \times \mathcal{V}(\mathbf{r} - \mathbf{r}') \cos \theta' \cos \theta, \quad (18)$$

$$\cos \theta = \hat{\mathbf{n}} \cdot \frac{(\mathbf{r}' - \mathbf{r})}{|\mathbf{r}' - \mathbf{r}|}, \quad \cos \theta' = \hat{\mathbf{n}}' \cdot \frac{(\mathbf{r} - \mathbf{r}')}{|\mathbf{r} - \mathbf{r}'|}.$$

In Eq. (18), $\mathcal{V}(\mathbf{r} - \mathbf{r}')$ is a visibility factor, which is either unity if both points \mathbf{r} and \mathbf{r}' can be joined by a straight line without intersecting an interface (i.e., when

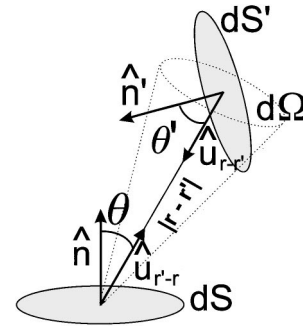


Fig. 2. Scheme for the solid-angle relationship between $d\mathbf{S} = \hat{\mathbf{n}} dS$ and $d\mathbf{S}' = \hat{\mathbf{n}}' dS'$.

they are visible to each other) or zero when such a straight line does not exist. From now on, and for the sake of simplicity, this factor will be implicitly assumed and therefore omitted.

An expression similar to that of Eq. (17) for the inward density flux can be found by means of Eq. (1) for the average intensity U_0 inside the nonscattering volume:

$$U_0(\mathbf{r}) = \int_S I_0(\mathbf{r}, \hat{\mathbf{u}}_{\mathbf{r}'-\mathbf{r}}) \frac{\mathbf{n}' \cdot \hat{\mathbf{u}}_{\mathbf{r}'-\mathbf{r}}}{|\mathbf{r} - \mathbf{r}'|^2} dS', \quad \mathbf{r} \in V, \quad (19)$$

which, with Eq. (14), can be rewritten as

$$U_0(\mathbf{r}) = \int_S I_0(\mathbf{r}', \hat{\mathbf{u}}_{\mathbf{r}'-\mathbf{r}}) \Gamma(\mathbf{r} - \mathbf{r}') dS', \quad \mathbf{r} \in V. \quad (20)$$

In Eq. (20), $\Gamma(\mathbf{r} - \mathbf{r}')$ is

$$\Gamma(\mathbf{r} - \mathbf{r}') = \frac{\exp[-\mu_{a0} |\mathbf{r} - \mathbf{r}'|]}{|\mathbf{r} - \mathbf{r}'|^2} \cos \theta'. \quad (21)$$

It must be stated that Eqs. (17) and (20) are general for the RTE, since no approximation has yet been imposed on I_0 .

B. Diffusion Approximation

Addressing once again the configuration depicted in Fig. 1, consider the case in which medium 1 is a strong scatterer with n_1 as index of refraction and μ_{a1} and μ_{s1} as absorption and scattering coefficients, respectively. These coefficients are such that $\mu_{s1} \gg \mu_{a1}$ so that the diffusion approximation to the RTE is now valid. In this case the main assumption is a first-order angular dependence of the specific intensity $I_1(\mathbf{r}, \hat{\mathbf{s}})$,³⁷

$$I_1(\mathbf{r}, \hat{\mathbf{s}}) = \alpha U_1(\mathbf{r}) + \beta \mathbf{J}_1(\mathbf{r}) \hat{\mathbf{s}}, \quad \mathbf{r} \in \tilde{V}, \quad (22)$$

where I_1 is the specific intensity, U_1 stands for the average intensity [see Eq. (1)], and \mathbf{J}_1 denotes the total density flux [see Eq. (2)] inside the diffusive medium. We find the values of α and β by applying Eqs. (1) and (2), thus obtaining $\alpha = 1/4\pi$ and $\beta = 3/4\pi$. The angular dependence of I_1 can be seen schematically in Fig. 3. Expression (22) also implies that at any point inside the diffusive medium, the total density flux is governed by Fick's law (see Ref. 37 for a detailed derivation),

$$\mathbf{J}_1(\mathbf{r}) = -\frac{1}{3(\mu'_{s1} + \mu_{a1})} [\nabla U_1(\mathbf{r}) - \mathbf{Q}_1(\mathbf{r})], \quad \mathbf{r} \in \tilde{V}, \quad (23)$$

where $D_1 = [3(\mu'_{s1} + \mu_{a1})]^{-1}$ is the diffusion coefficient (measured in centimeters), $\mu'_{s1} = (1 - g)\mu_{s1}$ is the reduced scattering coefficient, and g is the average cosine of the scattering angle.³⁷ In Eq. (23) the term \mathbf{Q}_1 takes care of the anisotropy and is defined in terms of the angular-dependent photon source ϵ (see Sec. 9-2 of Ref. 37) as

$$\mathbf{Q}_1(\mathbf{r}) = \int_{4\pi} \epsilon(\mathbf{r}, \hat{\mathbf{s}}) \hat{\mathbf{s}} d\Omega, \quad (24)$$

where ϵ is the power radiated by the source per unit volume per unit solid angle in the direction $\hat{\mathbf{s}}$. However, as will be shown, the derivation of the boundary conditions is in terms of $J_{n1} = \mathbf{J}_1 \cdot \hat{\mathbf{n}}$ and therefore is independent of the expression used for J_{n1} .

To find an expression similar to Eq. (17) for the non-scattering medium, we must make use of the value of I_1 at the interface. To this end, Eq. (23) can be rewritten as

$$\mathbf{J}_1 = J_{n1} \hat{\mathbf{n}} + J_{t1} \hat{\mathbf{t}}, \quad (25)$$

where $\hat{\mathbf{n}}$ and $\hat{\mathbf{t}}$ are the surface normal and the tangential unit vector, respectively. Introducing Eq. (22) into Eq. (11), making use of Eq. (25), we obtain

$$\begin{aligned} J^+(\mathbf{r}) = & \int_{(2\pi)^-} \frac{U_1(\mathbf{r})}{4\pi} [1 - |R_{1 \rightarrow 0}(\theta)|^2] \cos \theta d\Omega \\ & + \int_{(2\pi)^-} \frac{3J_{n1}(\mathbf{r})}{4\pi} [1 - |R_{1 \rightarrow 0}(\theta)|^2] \cos^2 \theta d\Omega, \end{aligned} \quad (26)$$

where the contribution from J_{t1} is zero, owing to the $\hat{\mathbf{s}} \cdot \hat{\mathbf{n}}$ factor in Eq. (11). Since the total flux density [see Eq. (3)] through the surface must be constant, we also obtain the relationship

$$J_n(\mathbf{r}) = J_{n1}(\mathbf{r}) = J_{n0}(\mathbf{r}), \quad (27)$$

where J_{n1} inside the diffusive medium is [see Eq. (23)]

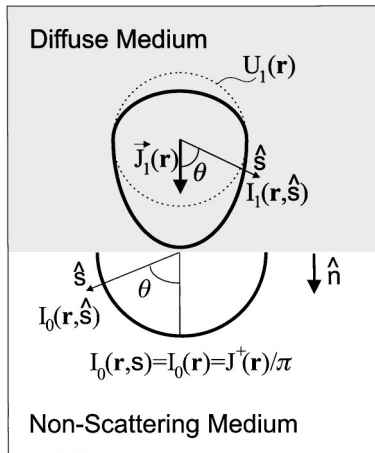


Fig. 3. Scheme for the specific intensities inside the diffusive medium and emerging into the non-scattering medium. Note the angular dependence to first order of I_1 in the diffusive medium, whereas in the non-scattering medium I_0 is angle independent. The light distribution radiated into the non-scattering medium, i.e., $I_0(\mathbf{r})$, gives rise to Lambert's power law: $dP(\mathbf{r}) = I_0(\mathbf{r}) \cos \theta dS$.

$$\begin{aligned} J_{n1}(\mathbf{r}) = & -D_1[\hat{\mathbf{n}} \cdot \nabla U_1(\mathbf{r}) - \hat{\mathbf{n}} \cdot \mathbf{Q}_1(\mathbf{r})] \\ = & -D_1 \frac{\partial U_1(\mathbf{r})}{\partial \hat{\mathbf{n}}} + D_1 \hat{\mathbf{n}} \cdot \mathbf{Q}_1(\mathbf{r}). \end{aligned} \quad (28)$$

Since \mathbf{J}_{n1} is defined as an integral over all possible angles [see Eq. (3)], neither U_1 nor J_{n1} has angular dependence. Therefore, with $d\Omega = 2\pi d(\cos \theta)$, Eq. (26) can be rewritten as

$$J^+(\mathbf{r}) = R_U \frac{U_1(\mathbf{r})}{2} + R_J \frac{J_{n1}(\mathbf{r})}{2}, \quad \mathbf{r} \in S, \quad (29)$$

where

$$\begin{aligned} R_U = & \int_0^1 [1 - |R_{0 \rightarrow 1}(\theta)|^2] \cos \theta d(\cos \theta), \\ R_J = & 3 \int_0^1 [1 - |R_{0 \rightarrow 1}(\theta)|^2] \cos^2 \theta d(\cos \theta). \end{aligned} \quad (30)$$

Relation (27) has been employed in Eq. (29) and will be used from now on. A detailed derivation of these equations can be found in Refs. 33 and 44.

3. BOUNDARY CONDITIONS

Equation (17) gives us the expression for the inward flux in terms of the specific intensity inside the non-scattering medium, whereas Eq. (29) gives us the expression for the outward flux in terms of the average intensity and density flux inside the diffusive medium. What is needed at this point is a boundary condition for the light wave that matches both media. The simplest approximation, which will be used throughout this paper, is to consider the light that is isotropically radiated from the diffusive medium (see Fig. 3). This involves the assumption that the specific intensity, radiated from the surface S into the non-scattering medium, will not have an angular dependence. Then, since the total flux that emerges from a point in the surface \mathbf{r} is J^+ , the specific intensity inside the non-scattering medium I_0 must be expressed as

$$I_0(\mathbf{r}, \hat{\mathbf{s}}) = I_0(\mathbf{r}) = \alpha J^+(\mathbf{r}), \quad (31)$$

where α is a constant. Since the total flux radiated into the non-scattering medium must be J^+ , by means of Eq. (6) we obtain $\alpha = 1/\pi$. Therefore, the power radiated into the non-scattering medium from a certain point \mathbf{r} of the surface element dS will be [see Eq. (4)]

$$dP(\mathbf{r}, \theta) = I_0(\mathbf{r}) \cos \theta dS d\Omega = \frac{J^+(\mathbf{r})}{\pi} \cos \theta dS d\Omega, \quad (32)$$

and the total power emitted from dS into the non-scattering medium would be

$$dP(\mathbf{r}) = \frac{1}{\pi} \int_{(2\pi)^+} J^+(\mathbf{r}) \cos \theta dS d\Omega = J^+(\mathbf{r}) dS. \quad (33)$$

Equation (32) is Lambert's cosine law⁴⁵ and is frequently used for describing light emerging from a strongly scattering medium, the surface boundary S acting as a secondary source (see Fig. 3). Substituting Eq. (31) into Eq. (17), we obtain the following expression for the total downward flux:

$$J^-(\mathbf{r}) = \frac{1}{\pi} \int_S J^+(\mathbf{r}') \mathcal{G}(\mathbf{r} - \mathbf{r}') dS', \quad \mathbf{r} \in S. \quad (34)$$

The total flux going into the diffusive medium is therefore a superposition of all outwardgoing fluxes at the surface S that are transmitted at point \mathbf{r} (see Fig. 2).

Therefore the total normal flux, $J_n = J^+ - J^-$, is

$$\begin{aligned} J_n(\mathbf{r}) &= R_U \frac{U_1(\mathbf{r})}{2} + R_J \frac{J_n(\mathbf{r})}{2} \\ &\quad - \frac{1}{\pi} \int_S \left[R_U \frac{U_1(\mathbf{r}')}{2} + R_J \frac{J_n(\mathbf{r}')}{2} \right] \\ &\quad \times \mathcal{G}(\mathbf{r} - \mathbf{r}') dS', \quad \mathbf{r} \in S. \end{aligned} \quad (35)$$

Grouping terms, we then obtain that

$$\begin{aligned} U_1(\mathbf{r}) &= C_n J_n(\mathbf{r}) + \frac{1}{\pi} \int_S \left[U_1(\mathbf{r}') + \frac{R_J}{R_U} J_n(\mathbf{r}') \right] \\ &\quad \times \mathcal{G}(\mathbf{r} - \mathbf{r}') dS', \quad \mathbf{r} \in S, \end{aligned} \quad (36)$$

where $C_n = (2 - R_J)/R_U$, as shown in Refs. 33 and 44. Equation (36) is the nonlocal boundary condition that we were seeking for light propagation in diffusive media with nonscattering regions. It must be stated that this boundary condition cannot take into account multiple reflections inside the nonscattering region when dealing with index-mismatched media. In the case of a plane interface (i.e., an open surface) there is only outgoing flux, and we recover the expression for the boundary condition in the diffusion approximation^{33,37}:

$$U_1(\mathbf{r}) = C_n J_n(\mathbf{r}), \quad \mathbf{r} \in S. \quad (37)$$

We wish to emphasize that more accurate values of C_n beyond the diffusion approximation can be found in the literature^{26,33} for some practical situations in which the solution reached by using Eq. (37) is not accurate enough. Even so, this is still an active field of research, and new methods to overcome this problem are needed.

The average intensity inside the nonscattering medium, Eq. (20), in this diffusion approximation case can be rewritten with the aid of Eq. (31) as

$$U_0(\mathbf{r}) = \frac{1}{\pi} \int_S J^+(\mathbf{r}') \Gamma(\mathbf{r} - \mathbf{r}') dS', \quad \mathbf{r} \in V. \quad (38)$$

At this point it must be underlined that Eqs. (36) and (38) have been derived for a three-dimensional configuration. The expressions for these equations in two dimensions can be found in Appendix A and are those that will be employed in our numerical simulations. Whenever dealing with non three-dimensional configurations, great care must be taken with the RTE, since conversion from three to two dimensions is nontrivial. A first-order approximation to Eq. (36) was used in Refs. 21 and 22 to deal with nonscattering regions in diffusive media for the index-matched case. This approximation consisted of applying the boundary condition Eq. (37) and including a secondary source at the interface given by

$$U^{(\text{sec})}(\mathbf{r}) = \frac{1}{\pi} \int_S J_n^{(0)}(\mathbf{r}') \mathcal{G}(\mathbf{r} - \mathbf{r}') dS', \quad \mathbf{r} \in S, \quad (39)$$

where $J_n^{(0)}$ denotes the zeroth-order approximation to the total flux, i.e., $J_n^{(0)} = U/C_n$. The main assumption that this approximation makes is that the total normal flux is equal to the total outward flux, i.e.,

$$J_n^{(0)}(\mathbf{r}) \simeq J^+(\mathbf{r}) = R_U \frac{U_1(\mathbf{r})}{2} + R_J \frac{J_n^{(0)}(\mathbf{r})}{2}, \quad \mathbf{r} \in S, \quad (40)$$

which gives the boundary condition $C_n J_n^{(0)} = U_1$. This approximation is expected to break down when the total inward flux is not small, but as shown in Refs. 21 and 22, it yields accurate results with biological parameters and will be employed in Section 4 with the FEM model. Also, whenever dealing with great differences in the refractive indices, both Eqs. (36) and (40) are expected to break down, since they cannot account for multiple reflections inside the nonscattering medium. That is, both Eqs. (36) and (40) deal with transmitted light and do not consider the reflected part, which would give rise to nonlinear equations.

A. Scattering Integral Equations

Let us address the scattering configuration depicted in Fig. 4. An infinite homogeneous diffusive medium of volume \tilde{V} with diffusion coefficient D_1 , absorption coefficient μ_{a1} , and refractive index n_1 , contains a nonscattering object of volume V , with absorption coefficient μ_{a0} and index of refraction n_0 , delimited by the surface S . Assuming the photon source located at $\mathbf{r}_{\text{source}}$ inside \tilde{V} and modulated by a frequency ω , the average intensity $U_1(\mathbf{r}, t) = U_1(\mathbf{r}) \exp(-i\omega t)$ is governed by the diffusion equation in the frequency domain, which can be expressed in \tilde{V} as^{2,38}

$$\nabla^2 U_1(\mathbf{r}) + \kappa_1^2 U_1(\mathbf{r}) = -\frac{S_0(\mathbf{r})}{D_1} - \nabla \cdot \mathbf{Q}_1(\mathbf{r}), \quad \mathbf{r} \in \tilde{V}. \quad (41)$$

Equation (41) is derived from current conservation.³⁷ S_0 is the source strength defined as [see Eq. (24)]

$$S_0(\mathbf{r}) = \int_{4\pi} \epsilon(\mathbf{r}, \hat{\mathbf{s}}) d\Omega \quad (42)$$

and represents the power generated per unit volume (watts per inverse centimeters cubed). D_1 is the diffusion coefficient previously defined. It must be stated that when we are dealing with an isotropic source, the term $\mathbf{Q}_1 = 0$. The complex diffusion wave number κ_1 is

$$\kappa_1^2 = -\frac{\mu_{a1}}{D_1} + i \frac{\omega n_1}{c D_1}, \quad (43)$$

c being the speed of light in vacuum. In Eq. (41) we have neglected the term $\nabla D_1(\mathbf{r}) \cdot \nabla U_1(\mathbf{r})/D_1(\mathbf{r})$ (see Ref. 38), since we consider the case in which both D_1 and μ_{a1} are constant throughout the diffusive medium (i.e., excluding the nonscattering regions). The Green's function $G(\kappa_1|\mathbf{r} - \mathbf{r}'|)$ corresponding to the diffusive medium satisfies

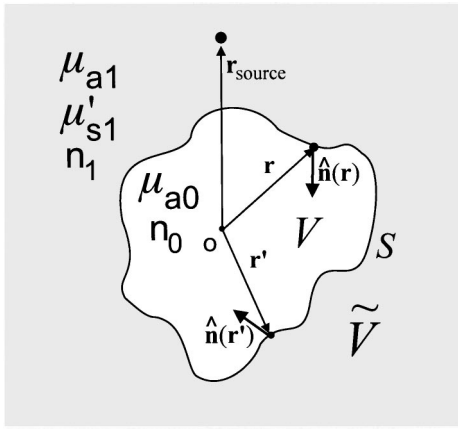


Fig. 4. Scattering geometry of a nonscattering region embedded in a diffusive medium.

$$\nabla^2 G(\kappa_1|\mathbf{r} - \mathbf{r}'|) + \kappa_1^2 G(\kappa_1|\mathbf{r} - \mathbf{r}'|) = -4\pi\delta(\mathbf{r} - \mathbf{r}'),$$

$$\mathbf{r}, \mathbf{r}' \in \tilde{V}, \quad (44)$$

and its expression is^{40,46,47}

$$G(\kappa_1|\mathbf{r} - \mathbf{r}'|) = \exp[i\kappa_1|\mathbf{r} - \mathbf{r}'|]/|\mathbf{r} - \mathbf{r}'|.$$

Inside the nonscattering volume V , the solution of Eq. (14) in the case of a modulated source with frequency ω is

$$I_0(\mathbf{r}, \hat{\mathbf{u}}_{r-r'}) = I_0(\mathbf{r}', \hat{\mathbf{u}}_{r-r'})$$

$$\times \exp\left[\left(-\mu_{a0} + i\frac{\omega n_0}{c}\right)|\mathbf{r} - \mathbf{r}'|\right],$$

$$\mathbf{r}, \mathbf{r}' \in V, \quad (45)$$

and the average intensity inside V is [see Eq. (38)]

$$U_0(\mathbf{r}) = \frac{1}{\pi} \int_S \left[\frac{R_U}{2} U_1(\mathbf{r}') + \frac{R_J}{2} J_n(\mathbf{r}') \right] \Gamma_\omega(\mathbf{r} - \mathbf{r}') dS',$$

$$\mathbf{r} \in V,$$

$$\Gamma_\omega(\mathbf{r} - \mathbf{r}') = \frac{\exp\{[-\mu_{a0} + i(\omega n_0/c)]|\mathbf{r} - \mathbf{r}'|\}}{|\mathbf{r} - \mathbf{r}'|^2} \cos \theta'. \quad (46)$$

By means of Eq. (46) we are able to find the average intensity at any point inside the nonscattering volume V .

Since the total density flux is governed by Fick's law [Eq. (23)] at the surface S , then, according to Eqs. (23), (27), and (28), $J_n(\mathbf{r}) = -D_1 \partial U_1(\mathbf{r}) / \partial \hat{\mathbf{n}} + D_1 \hat{\mathbf{n}} \cdot \mathbf{Q}_1(\mathbf{r})$. In this case Green's theorem,⁴⁶

$$\int_{\tilde{V}} (U_1 \nabla^2 G - G \nabla^2 U_1) d^3r = \int_{\tilde{S}} (U_1 \nabla G - G \nabla U_1) \cdot d\mathbf{s},$$

for the diffusive medium can be rewritten as

$$\int_{\tilde{V}} (U_1 \nabla^2 G - G \nabla^2 U_1) d^3r$$

$$= \int_S \left[U_1 \frac{\partial G}{\partial \hat{\mathbf{n}}} + G \left(\frac{J_n}{D_1} + \hat{\mathbf{n}} \cdot \mathbf{Q}_1 \right) \right] dS. \quad (47)$$

Multiplying Eq. (41) by G , Eq. (44) by U , subtracting both, performing an integral over the volume \tilde{V} , and ap-

plying Green's theorem [Eq. (47)], we obtain the following coupled integral equations for the diffusive medium^{40,46,47}:

$\mathbf{r}, \mathbf{r}' \in \tilde{V}$:

$$U_1(\mathbf{r}) = U^{(\text{inc})}(\mathbf{r}) + \Sigma_Q(\mathbf{r}) + \frac{1}{4\pi}$$

$$\times \int_S \left[U_1(\mathbf{r}') \frac{\partial G(\kappa_1|\mathbf{r} - \mathbf{r}'|)}{\partial \mathbf{n}'} \right.$$

$$\left. + G(\kappa_1|\mathbf{r} - \mathbf{r}'|) \frac{J_n(\mathbf{r}')}{D_1} \right] dS', \quad (48)$$

$\mathbf{r} \in V, \mathbf{r}' \in \tilde{V}$:

$$0 = U^{(\text{inc})}(\mathbf{r}) + \Sigma_Q(\mathbf{r})$$

$$+ \frac{1}{4\pi} \int_S \left[U_1(\mathbf{r}') \frac{\partial G(\kappa_1|\mathbf{r} - \mathbf{r}'|)}{\partial \mathbf{n}'} \right.$$

$$\left. + G(\kappa_1|\mathbf{r} - \mathbf{r}'|) \frac{J_n(\mathbf{r}')}{D_1} \right] dS', \quad (49)$$

where we have denoted the incident field intensity $U^{(\text{inc})}$ as

$$U^{(\text{inc})}(\mathbf{r}) = -\frac{1}{4\pi} \int_{\tilde{V}} \left[\frac{S_0(\mathbf{r}')}{D_1} + \nabla \cdot \mathbf{Q}_1(\mathbf{r}') \right]$$

$$\times G(\kappa_1|\mathbf{r} - \mathbf{r}'|) d\mathbf{r}' \quad (50)$$

and the contribution of the source anisotropy at the boundary, Σ_Q as

$$\Sigma_Q(\mathbf{r}) = \frac{1}{4\pi} \int_S \left[\frac{\hat{\mathbf{n}} \cdot \mathbf{Q}_1(\mathbf{r}')}{D_1} \right] G(\kappa_1|\mathbf{r} - \mathbf{r}'|) dS'. \quad (51)$$

The nonlocal boundary condition between the two media, Eq. (36), is

$$U_1(\mathbf{r}) = C_n J_n(\mathbf{r}) + \frac{1}{\pi} \int_S \left[U_1(\mathbf{r}') + \frac{R_J}{R_U} J_n(\mathbf{r}') \right]$$

$$\times \mathcal{G}_\omega(\mathbf{r} - \mathbf{r}') dS', \quad \mathbf{r} \in S,$$

$$\mathcal{G}_\omega(\mathbf{r} - \mathbf{r}') = [1 - |R_{0 \rightarrow 1}(\theta)|^2] \Gamma_\omega(\mathbf{r} - \mathbf{r}') \cos \theta. \quad (52)$$

Equations (48)–(52) constitute a closed set of integral equations that can be solved numerically for both U_1 and J_n . An exact procedure to solve this type of equation in arbitrary diffuse–diffuse interfaces is the extinction theorem (ET) method, which can be found in Ref. 38. Its use for diffusive media with index mismatch is reported in Ref. 44. The method has also been used extensively in electromagnetic scattering, and further references can be found in Refs. 39 and 40. Its use in other areas of research can be found in Ref. 48, where it is referred to as the boundary-element method.

Once the values of U_1 and J_n are found by solving Eqs. (48) and (52), U_1 and U_0 can be univocally determined at any point inside both the diffusive and the nonscattering medium by means of Eqs. (48) and (46), respectively. It should also be remarked that by similar arguments (see Ref. 38 and references therein), the above equations can

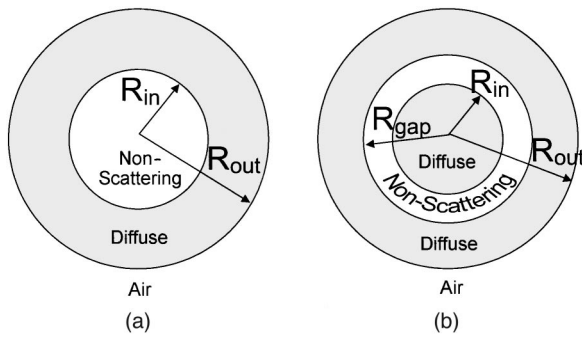


Fig. 5. Cases considered: (a) nonscattering cylinder of radius R_{in} embedded in a diffusive cylinder of radius R_{out} , (b) nonscattering gap of inner radius R_{in} and outer radius R_{gap} embedded in a diffusive cylinder of radius R_{out} .

be straightforwardly generalized to cases in which there are several nonscattering regions embedded in the diffusive medium, no matter whether these regions are rough or of any other arbitrary shape. Also, as in the case solved numerically in Section 4, the volume \tilde{V} can be bounded from the outside by a nonscattering medium: Actually, this would represent the more realistic case of a diffusive object surrounded by air with a nonscattering region embedded within (see Fig. 5).

4. NUMERICAL RESULTS

To assess the validity of the boundary condition [Eq. (36)], we study the two-dimensional configurations depicted in Fig. 5, where an outer cylinder of fixed radius $R_{out} = 2.5$ cm, filled with a diffusive medium of parameters $\mu'_{s1} = 20$ cm $^{-1}$ and $\mu_{a1} = 0.1$ cm $^{-1}$, is surrounded by air. We shall consider two cases: one in which a nonscattering cylinder of radius R_{in} is included [Fig. 5(a)] and another in which there is a nonscattering gap of outer radius R_{gap} and inner radius R_{in} between two diffusive regions [Fig. 5(b)]. In both cases the absorption coefficient for the nonscattering region is $\mu_{a0} = 0.05$ cm $^{-1}$. The speed of light is constant throughout the media, with refractive index $n_0 = n_1 = 1.4$. A continuous isotropic point source ($\omega = 0$) is placed at one transport mean free path $l_{tr} = 3D_1 \approx 0.05$ cm from the outer surface within the diffusive medium (i.e., $r_{source} = (R_{out} - l_{tr}) \approx 2.45$ cm). To quantify the limits of validity of the boundary condition, we shall consider several object sizes. For small objects, we must always take into consideration that for the diffusion approximation to remain valid, light must travel at least a few mean free paths. As shown in Ref. 13, on comparison with a Monte Carlo result, sizes smaller than or equal to the mean free path start causing deviations.

To permit reaching numerical convergence with the ET method, all surfaces have a discretization $dS = 0.025$ cm. The numerical calculations took 3 min for Fig. 5(a) and 9 min for Fig. 5(b) on a 200-MHz personal computer with a 128-Mb RAM. When the FEM was used, the mesh had between 949 nodes, 1614 elements ($R_{in} = 2$ cm) and 2323 nodes, 4456 elements ($R_{in} = 0.25$ cm) for the case in Fig. 5(a) and ≈ 2000 nodes and ≈ 4000 linear elements for the case in Fig. 5(b) (exact

numbers were different for each position of the gap). Computation times were 5–20 s on a 450-MHz Pentium II. The FEM has been reported extensively for many cases,^{41–43} and with this particular configuration in Ref. 22. Therefore we shall not explain it here. The FEM method with the approximate boundary conditions has already been contrasted in Ref. 22 with the MC method and with a discrete ordinate transport code, showing very good agreement with both. To assess the accuracy of the calculations performed with the ET and the FEM, we compared them with results from MC simulations. The description of the MC method for photon diffusion is well known (see, for example, Refs. 49 and 50) and will not be described here. The program is the same as that used in Ref. 22. 10^7 photons were launched during performance of the MC simulations. In all three methods the detector scanning was performed along the surface of the outer cylinder, i.e., at $r_{detec} = 2.5$ cm, with variation of the angular distance from the source. Once again, we note that when applying the ET model, we will use the complete boundary condition, Eq. (36), whereas when using the FEM method, we will use the approximate boundary condition, Eqs. (39) and (40). Also, whenever we were dealing with completely diffusive volumes, i.e., in the absence of the nonscattering region, the results from ET and FEM agreed to a high degree, thus implying that any differences the two methods may present with dealing with nonscattering volumes are due solely to the difference in the boundary conditions applied.

Figure 6 shows the results for the MC, FEM, and ET

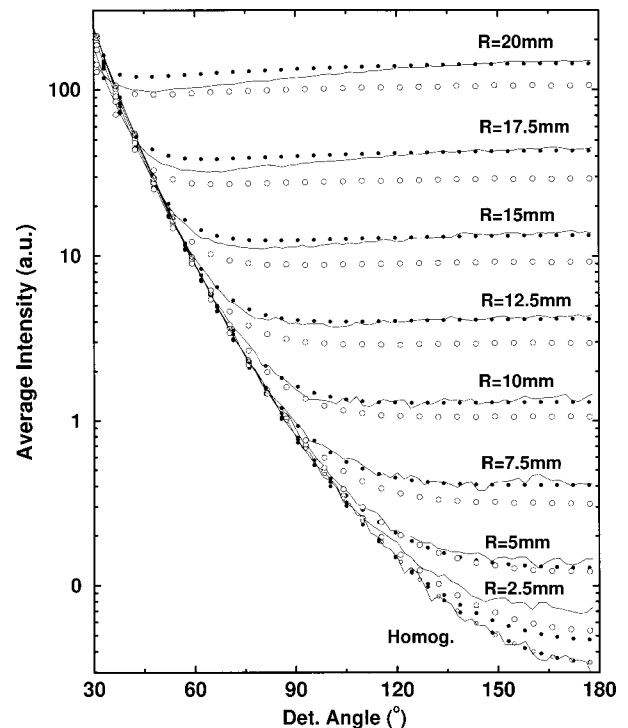


Fig. 6. Average intensity measured on the outer surface $R_{out} = 2.5$ cm versus detector angle separation, for the configuration depicted in Fig. 5(a). Values of $R_{in} = 0.25, 0.5, 0.75, 1.0, 1.25, 1.5, 1.75,$ and 2.0 cm. Results are presented for simulations performed with MC (solid curve), FEM (\circ), and ET (\bullet). In all cases a dc source ($\omega = 0$) was located at $r_{source} = 2.45$ cm at $\theta = 0$. $\mu_{a0} = 0.05$ cm $^{-1}$, $\mu_{a1} = 0.1$ cm $^{-1}$, $\mu_{s1} = 20$ cm $^{-1}$, $g = 0$.

calculations in the case represented in Fig. 5(a). R_{in} has been varied from $R_{in} = 0.25$ cm to $R_{in} = 2.0$ cm in 0.25-cm steps. This implies that the volume ratio of diffusive medium to total volume varies from $V_r = 36\%$ up to $V_r = 100\%$. As shown in Fig. 6, both FEM and the ET model account accurately for the photon transport in all cases, with ET being slightly more accurate. The reason for this difference is twofold: First, ET is an exact method, whereas FEM assumes an approximation on $\partial U/\partial x$. Second, the FEM uses the approximated boundary condition, Eqs. (39) and (40), whereas the ET is able to include the complete boundary condition, Eq. (36). As expected, results have a greater deviation from MC for greater values of R_{in} , i.e., for lower values of V_r . As a general rule, we may say that for values of $V_r > 75\%$ we obtain quite accurate results with both the FEM and the ET. Even so, results obtained for the case with $R_{in} = 2.0$ cm, i.e., $V_r = 36\%$, are quite impressive if we take into account that then 64% of the total volume is nonscattering. Also, if we look at the case with $R_{in} = 0.25$ cm, we see that there is a greater deviation than expected. The main reason for this is that such a small nonscattering volume stands in the limit of length scales within which the diffusion approximation works. That is, within the diffusion approximation context, in the same manner as diffusive regions with sizes of the order of l_{tr} can barely be considered actually diffusive (see Ref. 13), nonscattering objects with sizes of the order of l_{tr} embedded in diffusive media, can barely be considered to be actually nonscattering. Statistically this would mean that in a particular region of the diffusive object we have a lower concentration of scatterers, which, since the diffusion approximation always deals with averages, has a very low contribution. Thus, following these considerations, the results put forward by the FEM and ET methods for the case $R_{in} = 0.25$ cm show lower intensities (i.e., the nonscattering object is less visible) than those for the MC method.

In Fig. 7 we show the results for the MC, FEM, and ET calculations in the case represented in Fig. 5(b). Now we have considered two values of R_{in} , namely, $R_{in} = 1.0$ cm [Fig. 7(a)] and $R_{in} = 1.5$ cm [Fig. 7(b)]. For each value of R_{in} we computed five values of R_{gap} , which conferred the gap widths $W = R_{gap} - R_{in} = 0.1, 0.3, 0.5, 0.7,$ and 0.8 cm. In all cases we were always above a volume ratio $V_r > 75\%$, namely, between $V_r = 95\%$ ($W = 0.8$ cm) and $V_r = 99.84\%$ ($W = 0.1$ cm), so that a deviation due to low values of the volume ratio is not expected. As seen in Fig. 7, both the FEM and the ET show excellent agreement with MC. In this configuration, we once again reach more accurate results with the ET for high values of W , namely, $W = 3, 5, 7,$ and 8 mm, for the reason stated above. Also, a greater deviation of the ET occurs for smaller values of the gap width W , namely, $W = 0.1$ cm, in which cases the FEM yields better results. The reason for this is that this width is of the order of l_{tr} , and therefore the arguments that were applied to the case $R_{in} = 0.25$ cm of Fig. 6 can now be applied here. That is, when dealing with widths on the order of l_{tr} , the diffusion approximation fails and therefore the boundary conditions do not yield correct results. Also, since the FEM uses the approximate boundary condition, it appears that

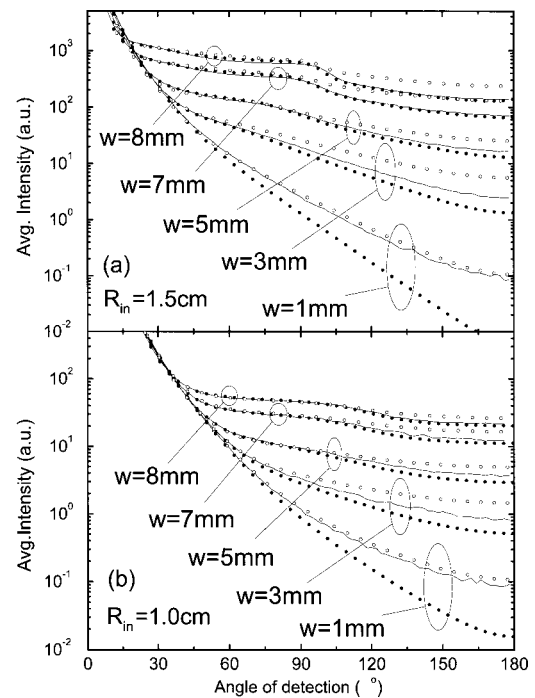


Fig. 7. Average intensity measured on the outer surface $R_{out} = 2.5$ cm versus detector angle separation, for the configuration depicted in Fig. 5(b). Values of (a) $R_{in} = 1.5$ cm, $R_{gap} = 1.6$ cm ($W = 0.1$ cm), 1.8 cm ($W = 0.3$ cm), and 2.0 cm ($W = 0.5$ cm). (b) $R_{in} = 1.0$ cm, $R_{gap} = 1.1$ cm ($W = 0.1$ cm), 1.3 cm ($W = 0.3$ cm), and 1.5 cm ($W = 0.5$ cm). Results are presented for simulations performed with MC (solid curve), FEM (\circ), and ET (\bullet). In all cases a dc source ($\omega = 0$) was located at $r_{source} = 2.45$ cm at $\theta = 0$. $\mu_{a0} = 0.05$ cm $^{-1}$, $\mu_{a1} = 0.1$ cm $^{-1}$, $\mu_{s1} = 20$ cm $^{-1}$, $g = 0$.

in cases of low values of $W \leq 3$ mm, the approximate boundary condition works better than the complete boundary condition. Also, on comparing the cases $W = 0.5, 0.7,$ and 0.8 cm from Figs. 7(a) and 7(b), we find that the depth of the gap buried in the diffusive medium, i.e., the value of R_{in} , does not change the accuracy of the results. We draw the attention to the curve corresponding to $W = 0.8$ cm in Fig. 7(a), where we find a sharp intensity decrease that is also predicted by the ET and the FEM (this effect was also found in Ref. 21, where it is referred to as a “kink”). This decrease in intensity appears when the inner diffusive volume, $\mathbf{r} \leq R_{in}$, is in the line of sight between source and detector, and its magnitude is greater the closer the outer radius R_{out} is from the source.

It is important to remark that what has been presented here corresponds to an *isotropic* point source. Whenever dealing with more realistic sources, such as a laser source impinging the diffusive object from outside, the light entering the diffusive region is *nonisotropic* at least within a few mean free paths, and the correct expression for \mathbf{Q}_1 must be included in Eq. (51). In any case, if the first non-diffuse interface, i.e., R_{gap} , is of the order of a few mean free paths l_{tr} near the source (typically $\sim 2l_{tr}$), the boundary condition Eq. (52) is expected to break down, since now light incident at the interface will no longer be well described by the diffusion approximation, Eq. (22) (see

Fig. 3). However, in the cases presented here the values of R_{gap} are such that they are located at least $4l_{\text{tr}}$ from the source, and as shown in Fig. 7(a) the diffusion approximation still accurately describes light transport.

5. CONCLUSIONS

In this paper we have studied the behavior of light transport when it encounters nonscattering regions in a diffusive medium. We have presented an expression for the average intensity inside both diffusive and nonscattering media and the matching across the interface separating both media. This expression gives rise to complete equations for the boundary conditions that model diffuse light in the presence of nonscattering regions. These expressions are rigorous within the diffusion approximation. We have presented an approximation to these boundary conditions that has already been employed in previous studies.^{21,22} To assess the validity of the boundary conditions, we have contrasted FEM and ET calculations with MC simulations. Due to the inherent structure of the FEM, the inclusion of the complete boundary condition is quite cumbersome, and hence the approximated expression has been used. On the other hand, ET calculations were possible with the complete boundary condition, and the corresponding integral equations were rigorously solved without any approximation. We have shown that both the ET with the complete boundary condition and the FEM with the approximate expression yield very good results when compared with MC, although slightly better agreement is reached with the ET. These calculations have been carried out for two different types of configurations: a nonscattering cylinder embedded in a diffusive cylinder and a nonscattering gap in a diffusive cylinder. We have demonstrated that both situations can be accurately modeled, and the limits of validity of the FEM and the ET have been established.

We stress, nevertheless, that the objective of this work is not to compare the FEM with the ET but rather to assess the validity of the boundary conditions put forward. Discussions of the relative advantages and disadvantages of the two methods can be found elsewhere,^{38,48} and have not been included here. Even so, we wish to state that the FEM requires less computational time than the ET, and therefore the ET is so far not useful with time-dependent equations. However the ET yields more accurate results, and complex boundary conditions can be included. On the other hand, the FEM, although not so accurate, is faster, and time dependence can be included without the need for a large amount of computing time. Therefore we suggest the use of ET to *assess* the accuracy of other faster methods, as has been done in this paper.

The modeling of nonscattering regions embedded within diffusive media is a subject of major interest, since a great deal of realistic media, such as the brain, includes them. We have presented here the boundary conditions that model such media, no matter the complexity of their surface geometry, and have studied their limits of validity. A subject that should be further addressed is the effect of index mismatch between the nonscattering regions and the surrounding diffusive media. As mentioned in Section 3, the limits of validity of the boundary conditions

presented in this paper are not clear in the case of index-mismatched media. This is an issue still under investigation.

APPENDIX A: BOUNDARY CONDITIONS IN TWO DIMENSIONS

The expressions for the boundary conditions in two dimensions are quite useful since the great majority of numerical simulations are performed in two dimensions because of their lower computational cost. Let us assume that in Fig. 2 the configuration is constant in the z direction. We write $\mathbf{r} = (\mathbf{R}, z)$, the unit normal $\hat{\mathbf{n}}(\mathbf{r}) = \hat{\mathbf{N}}(\mathbf{R})$, and the unit area as $d\mathbf{S} = d\mathbf{A}dz$. Since in this case U and J are z independent, we can rewrite Eq. (46) as

$$U_0(\mathbf{R}) = \frac{1}{\pi} \int_A J^+(\mathbf{R}') \Gamma_\omega^{2D}(\mathbf{R} - \mathbf{R}') dA', \quad (\text{A1})$$

$$\Gamma_\omega^{2D}(\mathbf{R} - \mathbf{R}') = \int_{-\infty}^{+\infty} \Gamma_\omega(\mathbf{r} - \mathbf{r}') dz'. \quad (\text{A2})$$

In Eq. (47), $\cos \theta'$ can be rewritten as $\cos \theta' = \cos \Theta' \cos \beta$, where $\cos \Theta' = \hat{\mathbf{u}}_{R-R'} \cdot \hat{\mathbf{N}}'$. With performance of the change of variable, $\cos \beta = R/\sqrt{R^2 + z^2}$, Eq. (A2) can be expressed as

$$\begin{aligned} \Gamma_\omega^{2D}(\mathbf{R} - \mathbf{R}') &= \frac{\hat{\mathbf{u}}_{R'-R} \cdot \hat{\mathbf{N}}}{|\mathbf{R} - \mathbf{R}'|} \\ &\times \int_{-\pi/2}^{\pi/2} \exp\left[-\mu_{a0} + i \frac{\omega n_0}{c} \frac{\mathbf{R} - \mathbf{R}'}{\cos \beta}\right] \\ &\times \cos \beta d\beta. \end{aligned} \quad (\text{A3})$$

Proceeding in a similar way, we obtain the following expression for the boundary condition Eq. (52):

$$\begin{aligned} U_1(\mathbf{R}) &= C_n J_n(\mathbf{R}) + \frac{1}{\pi} \int_A \left[U_1(\mathbf{R}') + \frac{R_J}{R_U} J_n(\mathbf{R}') \right] \\ &\times \mathcal{G}_\omega^{2D}(\mathbf{R} - \mathbf{R}') dA', \quad \mathbf{R} \in A, \end{aligned} \quad (\text{A4})$$

$$\mathcal{G}_\omega^{2D}(\mathbf{R} - \mathbf{R}') = \int_{-\infty}^{+\infty} \mathcal{G}_\omega(\mathbf{r} - \mathbf{r}') dz'. \quad (\text{A5})$$

Performing the same substitutions as in Eq. (A3), we obtain

$$\begin{aligned} \mathcal{G}_\omega^{2D}(\mathbf{R} - \mathbf{R}') &= \frac{(\hat{\mathbf{u}}_{R'-R} \cdot \hat{\mathbf{N}})(\hat{\mathbf{u}}_{R-R'} \cdot \hat{\mathbf{N}}')}{|\mathbf{R} - \mathbf{R}'|} \\ &\cdot \int_{-\pi/2}^{\pi/2} [1 - |R_{0 \rightarrow 1}(\theta^{(i)})|^2] \\ &\times \exp\left[-\mu_{a0} + i \frac{\omega n_0}{c} \frac{|\mathbf{R} - \mathbf{R}'|}{\cos \beta}\right] \\ &\times \cos^2 \beta d\beta, \end{aligned} \quad (\text{A6})$$

where $\cos \theta^{(i)} = \cos \beta \cos \Theta$. In the case in which there is no index mismatch, expression (A6) for \mathcal{G}_ω^{2D} can be approximated to

$$\mathcal{G}_\omega^{2D}(\mathbf{R} - \mathbf{R}') \approx \frac{\pi \cos \Theta \cos \Theta'}{2 |\mathbf{R} - \mathbf{R}'|} \times \exp\left[\left(-\mu_{a0} + i \frac{\omega n_0}{c}\right)|\mathbf{R} - \mathbf{R}'|\right]. \quad (\text{A7})$$

Expression (A7) is exact when $\omega = 0$, such as in the cases addressed in Refs. 21 and 22 and in the instances presented in this paper.

ACKNOWLEDGMENTS

We thank E. Okada and his group for help with the Monte Carlo code. This research has been supported by Comisi3n Interministerial de Ciencia y Tecnolog3a of Spain under grant PB98-0464 and by the Fundaci3n Ram3n Areces. J. Ripoll acknowledges a scholarship from Ministerio de Educaci3n y Cultura of Spain. S. R. Arridge and H. Dehghani thank the Wellcome Trust and the Engineering and Physical Sciences Research Council (UK).

The authors can be reached at the addresses on the title page or by e-mail: jripoll@icmm.csic.es, mnieto@icmm.csic.es, S. Arridge@cs.ucl.ac.uk, H. Dehghani@cs.ucl.ac.uk.

REFERENCES

1. E. B. de Haller, "Time-resolved transillumination and optical tomography," *J. Biomed. Opt.* **1**, 7–17 (1996).
2. A. Yodh and B. Chance, "Spectroscopy and imaging with diffusing light," *Phys. Today*, March 1995, pp. 38–40.
3. See related studies in *Advances in Optical Imaging and Photon Migration*, J. Fujimoto and M. S. Patterson, eds., Vol. 21 of Trends in Optics and Photonic Series (Optical Society of America, Washington, D.C., 1998).
4. S. R. Arridge, P. van der Zee, M. Cope, and D. T. Delpy, "Reconstruction methods for near infra-red absorption imaging," in *Time-Resolved Spectroscopy and Imaging of Tissues*, B. Chance and A. Katzir, eds., Proc. SPIE **1431**, 204–215 (1991).
5. M. A. O'Leary, D. A. Boas, B. Chance, and A. G. Yodh, "Experimental images of heterogeneous turbid media by frequency-domain diffusing-photon tomography," *Opt. Lett.* **20**, 426–428 (1995).
6. C. P. Gonatas, M. Ishii, J. S. Leigh, and J. C. Schotland, "Optical diffusion imaging using a direct inversion method," *Phys. Rev. E* **52**, 4361–4365 (1995).
7. Ch. L. Matson, N. Clark, L. McMackin, and J. S. Fender, "Three-dimensional tumor localization in thick tissue with the use of diffuse photon-density waves," *Appl. Opt.* **36**, 214–220 (1997).
8. X. D. Li, T. Durduran, A. G. Yodh, B. Chance, and D. N. Pattanayak, "Diffraction tomography for biochemical imaging with diffuse-photon density waves," *Opt. Lett.* **22**, 573–575 (1997).
9. S. A. Walker, S. Fantini, and E. Gratton, "Image reconstruction by backprojection from frequency-domain optical measurements in highly scattering media," *Appl. Opt.* **36**, 170–179 (1997).
10. H. Jiang, K. D. Paulsen, U. L. Osterberg, B. W. Pogue, and M. S. Patterson, "Simultaneous reconstruction of optical absorption and scattering maps in turbid media from near-infrared frequency-domain data," *Opt. Lett.* **20**, 2128–2130 (1995).
11. S. B. Colak, D. G. Papaioannou, G. W.'t Hooft, M. B. van der Mark, H. Schomberg, J. C. J. Paasschens, J. B. M. Melissen, and N. A. A. J. van Asten, "Tomographic image reconstruction from optical projections in light-diffusing media," *Appl. Opt.* **36**, 181–213 (1997).
12. P. N. den Outer, Th. M. Nieuwenhuizen, and A. Lagendijk, "Location of objects in multiple-scattering media," *J. Opt. Soc. Am. A* **10**, 1209–1218 (1993).
13. S. Feng, F. Zeng, and B. Chance, "Photon migration in the presence of a single defect: a perturbation analysis," *Appl. Opt.* **35**, 3826–3836 (1995).
14. S. R. Arridge and J. C. Hebden, "Optical imaging in medicine: II. Modeling and reconstruction," *Phys. Med. Biol.* **42**, 841–853 (1997).
15. J. C. Schotland, "Continuous-wave diffusion imaging," *J. Opt. Soc. Am. A* **14**, 275–279 (1997).
16. S. J. Norton and T. Vo-Dinh, "Diffraction tomographic imaging with photon density waves: an explicit solution," *J. Opt. Soc. Am. A* **15**, 2670–2677 (1998).
17. S. A. Walker, D. A. Boas, and E. Gratton, "Photon density waves scattered from cylindrical inhomogeneities: theory and experiments," *Appl. Opt.* **37**, 1935–1944 (1998).
18. S. Fantini, S. A. Walker, M. A. Franceschini, M. Kaschke, P. M. Schlag, and K. T. Moesta, "Assessment of the size, position, and optical properties of breast tumor *in vivo* by non-invasive optical methods," *Appl. Opt.* **37**, 1982–1989 (1998).
19. J. C. Hebden, F. E. W. Schmidt, M. E. Fry, M. Schweiger, E. M. C. Hillman, D. T. Delpy, and S. R. Arridge, "Simultaneous reconstruction of absorption and scattering images by multichannel measurement of purely temporal data," *Opt. Lett.* **24**, 534–536 (1999).
20. S. R. Arridge, "Optical tomography in medical imaging," *Topical Rev. Inverse Probl.* **15**, R41–R93 (1999).
21. M. Firbank, S. R. Arridge, M. Schweiger, and D. T. Delpy, "An investigation of light transport through scattering bodies with non-scattering regions," *Phys. Med. Biol.* **41**, 767–783 (1996).
22. S. R. Arridge, H. Dehghani, M. Schweiger, and E. Okada, "The finite element model for the propagation of light in scattering media: a direct method for domains with non-scattering regions," *Med. Phys.* **27**, 252–264 (2000).
23. S. Takahashi, D. Imai, and Y. Yamada, "Fundamental 3D FEM analysis of light propagation in head model toward 3D optical tomography," in *Optical Tomography and Spectroscopy of Tissue: Theory, Instrumentation, Model and Human Studies II*, Proc. SPIE **2979**, 130–138 (1997).
24. S. Takahashi and Y. Yamada, "Simulation of 3D light propagation in a layered head model including a clear CSF layer," in *Advances in Optical Imaging and Photon Migration*, J. Fujimoto and M. S. Patterson eds., Vol. 21 of Trends in Optics and Photonic Series (Optical Society of America, Washington, D.C., 1998).
25. M. S. Patterson, B. Chance, and B. C. Wilson, "Time resolved reflectance and transmittance for the noninvasive measurement of tissue optical properties," *Appl. Opt.* **28**, 2331–2336 (1989).
26. N. G. Chen and J. Bai, "Monte Carlo approach to modeling of boundary conditions for the diffusion equation," *Phys. Rev. Lett.* **80**, 5321–5324 (1998).
27. C. P. Gonatas, M. Miwa, M. Ishii, J. Schotland, B. Chance, and J. S. Leigh, "Effects due to geometry and boundary conditions in multiple light scattering," *Phys. Rev. E* **48**, 2212–2216 (1993).
28. I. Freund, "Surface reflections and boundary conditions for diffusive photon transport," *Phys. Rev. A* **45**, 8854–8858 (1992).
29. K. Furutsu, "Boundary conditions of the diffusion equation and applications," *Phys. Rev. A* **39**, 1386–1401 (1989).
30. J. Wu, F. Partovi, M. S. Field, and R. P. Rava, "Diffuse reflectance from turbid media: an analytical model of photon migration," *Appl. Opt.* **32**, 1115–1121 (1993).
31. S. Ito, "Diffusion of collimated, narrow beam waves in discrete random media," *Appl. Opt.* **34**, 7106–7112 (1995).
32. R. C. Haskell, L. O. Vaasand, T. Tsay, T. Feng, M. S. McAdams, and B. J. Tromberg, "Boundary conditions for the diffusion equation in radiative transfer," *J. Opt. Soc. Am. A* **11**, 2727–2741 (1994).
33. R. Aronson, "Boundary conditions for diffusion of light," *J. Opt. Soc. Am. A* **12**, 2532–2539 (1995).

34. D. J. Durian and J. Rudnick, "Spatially resolved backscattering: implementation of extrapolation boundary condition and exponential source," *J. Opt. Soc. Am. A* **16**, 837–844 (1999).
35. A. D. Kim and A. Ishimaru, "Optical diffusion of continuous-wave, pulsed, and density waves in scattering media and comparisons with radiative transfer," *Appl. Opt.* **37**, 5313–5319 (1998).
36. F. Martinelli, A. Sassaroli, G. Zaccanti, and Y. Yamada, "Properties of the light emerging from a diffusive medium: angular dependence and flux at the external boundary," *Phys. Med. Biol.* **44**, 1257–1275 (1999).
37. A. Ishimaru, *Wave Propagation and Scattering in Random Media* (Academic, New York, 1978), Vol. I.
38. J. Ripoll and M. Nieto-Vesperinas, "Scattering integral equations for diffusive waves. Detection of objects buried in diffusive media in the presence of rough interfaces," *J. Opt. Soc. Am. A* **16**, 1453–1465 (1999).
39. J. A. Sánchez-Gil and M. Nieto-Vesperinas, "Light scattering from random rough dielectric surfaces," *J. Opt. Soc. Am. A* **8**, 1270–1286 (1991).
40. A. A. Maradudin, T. Michel, A. R. McGurn, and E. R. Méndez, "Enhanced backscattering of light from a random grating," *Ann. Phys. (N.Y.)* **203**, 255–307 (1990).
41. S. R. Arridge, M. Schweiger, M. Hiraoka, and D. T. Delpy, "A finite element approach for modeling photon transport in tissue," *Med. Phys.* **20**, 299–309 (1993).
42. M. Schweiger, S. R. Arridge, M. Hirakoa, and D. T. Delpy, "The finite element model for the propagation of light in scattering media: boundary and source conditions," *Med. Phys.* **22**, 1779–1792 (1995).
43. S. R. Arridge, "Photon-measurement density functions. Part I: Analytical forms," *Appl. Opt.* **34**, 7395–7409 (1995).
44. J. Ripoll and M. Nieto-Vesperinas, "Index mismatch for diffuse photon density waves at both flat and rough diffuse-diffuse interfaces," *J. Opt. Soc. Am. A* **16**, 1947–1957 (1999).
45. M. Born and E. Wolf, *Principles of Optics*, 6th ed. (Pergamon, New York, 1993).
46. G. B. Arfken and H. J. Weber, *Mathematical Methods for Physicists*, 4th ed. (Academic, New York, 1995).
47. M. Nieto-Vesperinas, *Scattering and Diffraction in Physical Optics* (Wiley-Interscience, New York, 1991).
48. C. A. Brebbia and J. Dominguez, *Boundary Elements, An Introductory Course* (Computational Mechanics Publications, McGraw-Hill, New York, 1989).
49. L. H. Wang, S. L. Jacques, and L. Q. Zheng, "MCML-Monte Carlo modeling of photon transport in multilayered tissues," *Comput. Methods Programs Biomed.* **47**, 131–146 (1995).
50. R. Graaff, M. H. Koelink, F. F. M. de Mul, W. G. Zijlstra, A. C. M. Dassel, and J. G. Aarnoudse, "Condensed Monte Carlo simulations for the description of light transport," *Appl. Opt.* **32**, 426–434 (1993).